Journal of Alloys and Compounds 509 (2011) 542–545

Contents lists available at ScienceDirect

Journal of Alloys and Compounds

journal homepage: www.elsevier.com/locate/jallcom

First principle investigation of electronic structure of $CaMnO_3$ thermoelectric compound oxide

F.P. Zhang*, Q.M. Lu, X. Zhang, J.X. Zhang

Key Laboratory of Advanced Functional Materials, Chinese Ministry of Education, College of Material Science and Engineering, Beijing University of Technology, 100124, Beijing, People's Republic of China

ARTICLE INFO

Article history:
Received 17 July 2010
Received in revised form
14 September 2010
Accepted 18 September 2010
Available online 25 September 2010

Keywords:
First principle calculation
Perovskite thermoelectric $CaMnO_3$
Electronic structure

ABSTRACT

First principle calculations are employed to investigate the anti-ferromagnetic $CaMnO_3$ with regard to its geometry, ground state electronic structure and charge distributions. The G-type anti-ferromagnetic $CaMnO_3$ is found to be more stable via total energy minimization calculations; the calculated energy band structure reveals its band gap of 0.7 eV. There are combinations of light carriers in conduction bands and heavy carriers in valence bands that should favor high thermoelectric properties. The Mn*d* and O*p* orbitals are responsible for energy bands near Fermi level and they contribute to electronic property. There is strong hybridization between Mn*d* and O*p* orbitals and, the hybridization between Mn and O1 orbitals is stronger, it is indicated that the charge carriers are apt to transport along Mn–O1.

1. Introduction

Crisis between resource and ecology has been a motivity for human beings to find clean energy resolution urgently nowadays. Thermoelectric (TE) material affords a promising converter between heat energy and electrical energy directly and, the process is not harmful to the environment [1,2]. The efficiency of a TE generator depends on the material's TE dimensionless figure of merit ZT. The ZT is defined as $ZT = \alpha^2 T/\rho\kappa$, where α is thermopower, ρ is electrical resistivity, κ is total thermal conductivity and T is absolute temperature, respectively [2,3]. Applicable TE materials require high thermopower α, low resistivity ρ and total thermal conductivity κ. Good TE materials are typically regarded as heavily doped semiconductors with low thermal conductivity κ simultaneously providing a balance between the large thermopower α and low electrical resistivity ρ [4].

Transitional metal oxides have attracted much attention for their potential application [5–9]. Among these oxides, the manganese oxide $CaMnO_3$ with perovskite type crystal structure has received much interest in the past decade due to its structural [9], topological [10], physical [11], magnetical [12] and TE properties [9,13,14]. As for the TE property, the titled manganite exhibits both high thermopower α and relatively low total thermal conductivity κ above room temperature [9]. Furthermore, it has advantages such as no noxious gas emission, high temperature stability, cheap raw materials and easy fabrication comparing with conventional TE alloys. The $CaMnO_3$ oxide is very suitable for long-time use at high temperature in air for energy conversion and the TE properties could be further improved by doping [9,13–16]. The drawback of TE $CaMnO_3$ oxide might be its high electrical resistivity ρ comparing with traditional TE alloys. The electrical transport properties of $CaMnO_3$ can be intensively influenced by the oxygen deficiency, too [17–19]. Previous attention concerning $CaMnO_3$ manganite as for TE aspect has been paid on its crystal structure, temperature change induced phase transition, magnetic properties and doping properties [9,10,12,20]. The electrical properties are theoretically determined by the electronic structure; however detailed reports in terms of electronic structure, as well as relationship between electronic structure and TE properties are currently lacking.

First principle calculation within the framework of density functional theory (DFT) has been successfully applied in analyzing physical properties of materials [21–24]. In the present work, the constructed geometric structure is optimized by total energy minimization calculation, the G-type anti-ferromagnetic phase $CaMnO_3$ system is found to have lowest free energy, and it is thus subjected to electronic structure calculation. The relationship between geometric structure, composition, electronic structure and TE properties are analyzed based on results from DFT calculations for the first time to our knowledge.

2. Computational details

2.1. Theoretical model

The crystal structure of perovskite type $CaMnO_3$ with orthorhombic symmetry has been described and the atomic frac-

* Corresponding author. Tel.: +86 10 67392661; fax: +86 10 67392840.
E-mail addresses: zhfp@emails.bjut.edu.cn, zhfpeng@yahoo.com.cn (F.P. Zhang).

0925-8388/$ – see front matter © 2010 Elsevier B.V. All rights reserved.
doi:10.1016/j.jallcom.2010.09.102

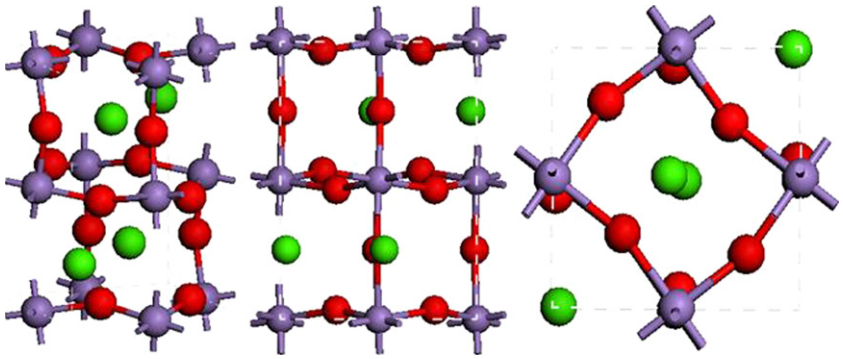

Fig. 1. Unit cell of orthorhombic $CaMnO_3$ (a) tridimensional view, (b) view from 0 0 1 direction and 0 1 0 direction (c). Red spheres represent O, deep blue spheres represent Mn and green spheres represent Ca. (For interpretation of the references to colour in this figure legend, the reader is referred to the web version of the article.)

Table 1
Lattice constants and atomic occupation site for $CaMnO_3$.

Lattice constants (experimental value and optimized value)			Space group
a	b	c	
5.2812 (5.3193)	7.4571 (7.4148)	5.2753 (5.2093)	pnma
α	β	γ	
90°	90°	90°	

Atom	x	y	z	Occupancy
Atomic occupation site				
Ca	0.0288 (6)	0.250	−0.008 (2)	1
Mn	0	0	0.5	1
O1	0.489 (2)	0.250	0.067 (3)	1
O2	0.285 (3)	0.033 (2)	0.711 (3)	1

tional coordinates were also determined in several reports. We applied cell parameters from Ref. [25] as lattice constants within our bulk material property calculation. Table 1 displays the lattice parameters and atomic occupation sites. Fig. 1 presents the schematic illustration for the unit cell with formula $Ca_4Mn_4O_{12}$. The anti-ferromagnetic aligned phase of our target system G-type $CaMnO_3$ is illustrated in Fig. 2 in which each Mn atom is surrounded by six Mn neighbors. In the present study, we have firstly attempted the full geometric optimization for the cell using total energy minimization method.

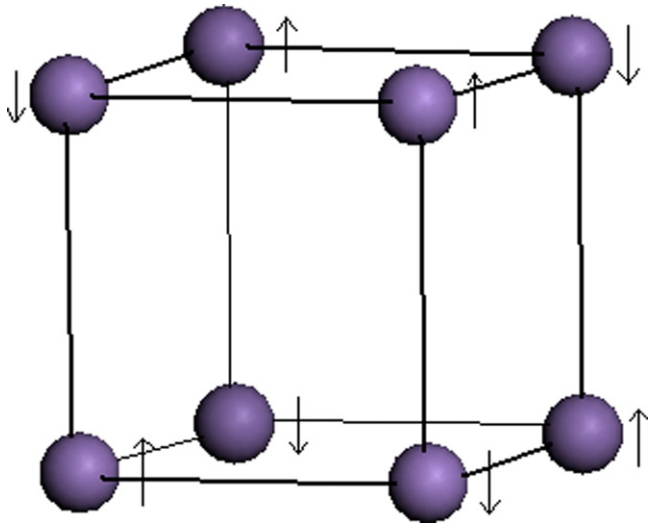

Fig. 2. The spin alignment of G-type anti-ferromagnetic structure for Mn atoms.

2.2. Calculation method

Calculations with the ultra-soft pseudo-potential plane wave method and generalized gradient approximations (GGA) based on DFT theory were performed using the Cambridge Serial Total Energy Package (CASTEP, Cerius2, Molecular Simulation, Inc.) [26]. Pseudo atomic calculation for Ca ($3s^2$ $3p^6$ $4s^2$), Mn ($3d^5$ $4s^2$) and O ($2s^2$ $2p^4$) was performed. The electron-ion interaction was described by a Vanderbilt's ultrasoft pseudo-potentials. The exchange correlation interaction energy was described using Perdew Burke Ernzerh functional within GGA framework. The atom positions were allowed to be optimized during the geometric optimization and the max displacement tolerance was set as 0.001 Å. In the total energy calculations, integrations over the Brillouin zone were performed for the unit cell. The valence electronic wave functions were expanded in a plane-wave basis set up to an energy cutoff of 340 eV, which converged the total energy of the unit cell to better than 0.01 meV/atom. In the electronic structure calculation, the Monkhorst-pack grid $5 \times 3 \times 5$ was used for k-point sampling; the band energy tolerance was set as 0.01 meV. Then the electronic structure was analyzed in terms of the band structure and density of states (DOS). The high symmetry k-points within our calculated band structure in the Brillouin zone were G(0.000, 0.000, 0.000), F(0.000, 0.500, 0.000), Q(0.000, 0.500, 0.500), Z(0.000, 0.000, 0.500).

3. Results and discussion

The manganite system $CaMnO_3$ is anti-ferromagnetic. In our investigation, the G-type anti-ferromagnetic phase $CaMnO_3$ system is found to have lowest free energy through the total energy minimization calculation for A-type and G-type anti-ferromagnetic phases; this indicates that the G-type anti-ferromagnetic phase $CaMnO_3$ system is more stable and, this type of anti-ferromagnetic alignment of Mn for many perovskite manganite materials is more stable. The deviations of obtained lattice constants are very low ($\leq$1.3%) and our optimization result is reasonable. The calculated energy band structure for the G-type anti-ferromagnetic phase $CaMnO_3$ system along a high symmetry direction in the Brillouin zone is shown in Fig. 3. The Fermi level is set to be 0 eV, other energy levels are determined comparing with Fermi level. The valence band maximum (VBM) and the conduction band minimum (CBM) at different points results in an indirect band gap material. Although the DFT calculation underestimates the band gap, the value of this gap turns out to be 0.7 eV and the band gap value accounts for its semiconductor behavior [27]. Since electrical transport properties are closely related to the electronic states near the highest valence band and the lowest conduction band for the titled compound, it is reasonable to focus on the energy bands near the Fermi level. The dispersion of top valence bands fluctuate with small energy

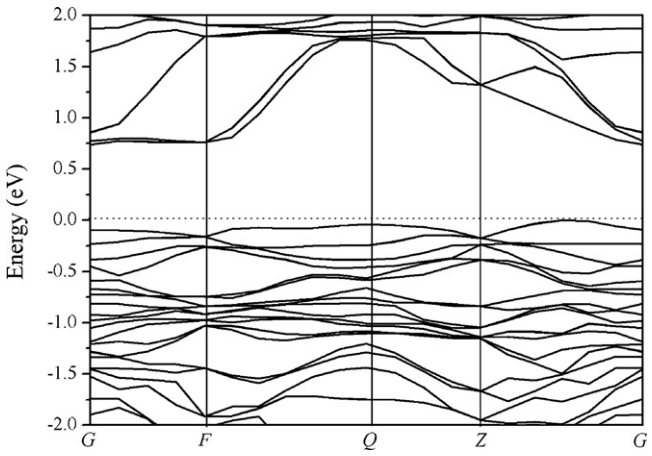

Fig. 3. Energy band structure of $CaMnO_3$.

region, we would see that these relatively heavy bands with large effective mass contribute to high thermopower. For materials with simple band structure, the absolute thermopower value α could be described proportional to:

$$\alpha \propto C\frac{k}{e}\ln\frac{(\pi m^* kT)^{3/2}}{nh^3} \quad (1)$$

where α is thermopower, k is Boltzmann constant, e is elementary charge, n is carrier density, h is Planck's constant, m^* is effective mass of charge carrier, C is an integrated constant and T is absolute temperature [28]. It can be evaluated that the large effective mass of the carrier contributes to the high thermopower of $CaMnO_3$, i.e. $\alpha = -800\ \mu VK^{-1}$ at 300 K [29]. There are also lighter bands near the lowest conduction band, this combination of heavy and light bands is often favorable for good TE materials as reported in filled skutterudite compound [30]. We would see together with the density of states that the Mn*d* and O*p* orbitals and their couplings are responsible for the bands near Fermi level and the high thermopower. The way to realize an applicable TE material consists in finding materials with low resistivity ρ; the reasonable mobility and carrier density can contribute to lower resistivity ρ. Consequently, doping that adjusts carrier density and carrier mobility can be positive [31–33].

Fig. 4 shows the calculated total partial density of states for $CaMnO_3$. It can be seen that the valence bands below Fermi energy

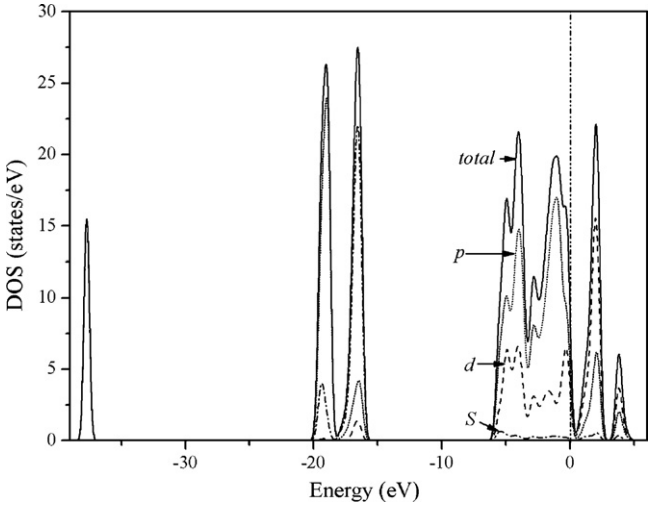

Fig. 4. Total partial density of states for $CaMnO_3$.

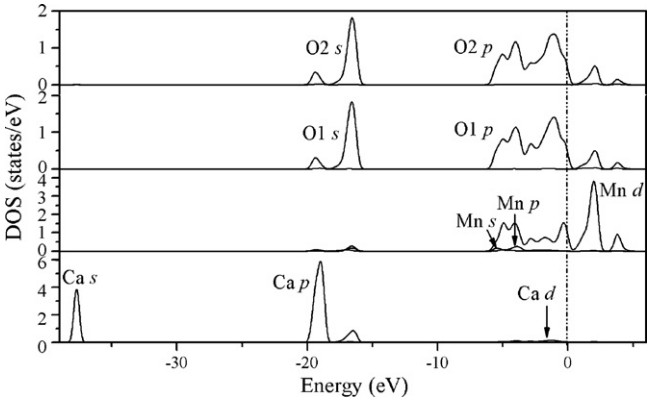

Fig. 5. Partial density of states of Ca, Mn and O atoms for $CaMnO_3$.

are dominated by the Mn*d* and O*p* orbitals with minor contributions of the other states of Ca forming the compound. The materials with high thermopower are usually associated with a large density of states near Fermi level. It can be seen that the large density of states near Fermi level of the titled manganite is also responsible for its high thermopower. Since the bands near VBM and the bands near CBM contribute to the electrical properties, the Mn*d* and O*p* electrons are inferred to play a main role in transportation process. This is in accordance with former reports [13–19]. As can be seen further at energy regions of −20 eV to −15 eV, −5 eV to 0 eV, 0 eV to 5 eV, there are high degree of hybridization between the Mn*d* and O*p* electrons. It is usually regarded that the polaron hopping governs the conduction process if the carrier transport in $CaMnO_3$ system can be considered as adiabatic [33–35]. It can be estimated hereby that the Mn*d* and O*p* orbitals are responsible for polaron hoping mechanism. The electron hops from its equilibrium site to nearest site by disturb caused by thermal potential or electrical field, and then a pair of polaron is formed (Fig. 5).

Since the O–Mn–O octahedron plays important role for its physical property, special attention is paid to the two kinds of oxygen of the octahedron. The first kind of oxygen is the four oxygens on the rectangular plane; the second kind of oxygen is the two oxygens at the octahedral poles. We denote them by O1 and O2 respectively to differentiate them, as shown in Fig. 6. It can be observed from the partial density of states of O1 and O2 that the two kinds of oxygen exhibit different hybridization behavior; this is verified by their charge distributions shown in Table 2. There are higher degree of hybridization between Mn and O1 than that between Mn and O2 near −3 eV, which indicates more charge carriers transport along Mn–O1 in conduction process. Our further transportation coefficients investigations [36] validate this estimation and the detailed results would be reported in succession.

It is proposed that the probable O vacancy occurs at the O1 site [10] for O reduced compounds during fabrication process of

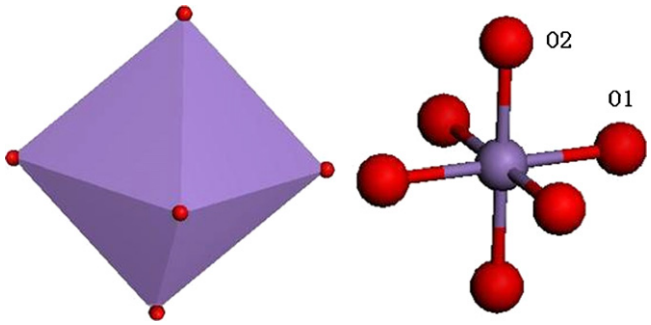

Fig. 6. Illustration of octahedron for $CaMnO_3$.

Table 2
Charge populations for species forming $CaMnO_3$.

Elements	Orbital				Charge
	s	*p*	*d*	Total	
Ca	2.11	5.99	0.65	8.75	1.25
Mn	0.28	0.58	5.47	6.34	0.66
O1	1.84	4.80	0	6.64	−0.64
O2	1.84	4.80	0	6.63	−0.63

$CaMnO_3$-based TE materials, this indicates that the formation of O reduction phase during the fabrication process of $CaMnO_3$ TE oxides would be deleterious. The O vacancy should be prohibited in sample preparation process. Our theoretical estimation agrees well with observations that the O vacancy for perovskite $CaMnO_3$ compound oxides deteriorates the electrical conduction capability [31,37,38].

4. Conclusions

In summary, the electronic structure of G-type anti-ferromagnetic $CaMnO_3$ has been studied; the relationship between its geometric structure, composition, electronic structure and TE properties has also been investigated. We find that the G-type anti-ferromagnetic phase $CaMnO_3$ has an indirect band gap of 0.7 eV interpreting its semiconductor behavior. The density of states near Fermi level is very high and is mainly composed of Mn*d* and O*p* electrons, these electrons are responsible for charge carrier transport process. The heavy bands and light bands near Fermi level are observed. The different kinds of oxygens are analyzed with regard to different electronic behaviors; more charge carriers conduction along Mn–O1 is observed. The O vacancy should be prohibited during fabrication process of $CaMnO_3$ TE materials.

Acknowledgements

This work is financially supported by National Natural Science Foundation of China under Grant Nos. 50702003 and 50801002.

References

[1] D. Tewelddebrhan, V. Goyal, A.A. Balandin, Nano Lett. 10 (2010) 1209.
[2] D. Kenfaui, D. Chateigner, M. Gomina, J.G. Noudem, J. Alloys Compd. 490 (2010) 472.
[3] F.P. Zhang, Q.M. Lu, J.X. Zhang, J. Alloys Compd. 484 (2009) 550.
[4] G.J. Snyder, M. Christensen, E. Nishibori, T. Caillat, B.B. Iversen, Nat. Mater. 3 (2004) 458.
[5] M. Karppinen, H. Fjellvag, T. Konno, Y. Morita, T. Motohashi, H. Yamauchi, Chem. Mater. 16 (2004) 2790.
[6] H. Ohta, K. Sugiura, K. Koumoto, Inorg. Chem. 47 (2008) 8429.
[7] E. Guilmeau, R. Funahashi, J. Appl. Phys. 85 (2004) 1490.
[8] K. Fujita, T. Mochida, K. Nakamura, Jpn. J. Appl. Phys. 40 (2001) 4644.
[9] L. Bocher, M.H. Aguirre, R. Robert, D. Logvinovich, S. Bakardjieva, J. Hejtmanek, A. Weidenkaff, Acta Mater. 57 (2009) 5667.
[10] K.R. Poeppelmeier, M.E. Leonowicz, J.C. Scanlon, J. Solid State Chem. 45 (1982) 71.
[11] D. Sousa, M.R. Nunes, C. Silveira, I. Matos, A.B. Lopes, M.E.M. Jorge, Mater. Chem. Phys. 109 (2008) 311.
[12] X.J. Fan, H. Koinuma, T. Hasegawa, Physica B 329–333 (2003) 723.
[13] N. Kumar, H. Kishan, A. Rao, V.P.S. Awana, J. Alloys Compd. 502 (2010) 283.
[14] Y. Wang, Y. Sui, P. Ren, L. Wang, X. Wang, W. Su, H. Fan, Inorg. Chem. 49 (2010) 3216.
[15] J.W. Park, D.H. Kwak, S.H. Yoon, S.C. Choi, J. Alloys Compd. 487 (2009) 550.
[16] R. Ang, Y.P. Sun, Y.Q. Ma, B.C. Zhao, X.B. Zhu, W.H. Song, J. Appl. Phys. 100 (2006) 063902.
[17] M.E. Melo Jorge, M.R. Nunes, R. Silva Maria, D. Sousa, Chem. Mater. 17 (2005) 2069.
[18] A. Reller, J.M. Thomas, D.A. Jefferson, M.K. Uppal, Proc. R. Soc. Lond. A 394 (1984) 223.
[19] E. Bakken, J. Boeiro-Goates, T. Grande, B. Hovde, T. Norby, L. Romark, Solid State Ionics 176 (2005) 2261.
[20] Q. Zhou, B.J. Kennedy, J. Phys. Chem. Solids 67 (2006) 1598.
[21] Y.S. Liu, Y.C. Chen, Phys. Rev. B 79 (2009) 193101.
[22] S. Baroni, P. Giannozzi, A. Testa, Phys. Rev. Lett. 58 (1987) 1861.
[23] S.H. Ke, W. Yang, S. Curtarolo, H.U. Baranger, Nano Lett. 9 (2009) 1011.
[24] N.J. English, J.S. Tse, Phys. Rev. Lett. 103 (2009) 015901.
[25] I. Gil de Muro, M. Insausti, L. Lezama, T. Rojo, J. Solid State Chem. 178 (2005) 928.
[26] M.C. Payne, M.P. Teter, D.C. Allan, T.A. Arias, J.D. Joannopou los, Rev. Modern Phys. 64 (1992) 1045.
[27] M. Matsukawa, A. Tamura, Y. Yamato, T. Kumagai, S. Nimori, R. Suryanarayanan, J. Magn. Magn. Mater. 310 (2007) e283.
[28] T. Tsubota, T. Ohno, N. Shiraishi, Y. Miyazaki, J. Alloys Compd. 463 (2008) 288.
[29] M. Miclau, Hébert, R. Retoux, C. Martin, J. Solid State Chem. 178 (2005) 1104.
[30] L. Zhang, D.J. Singh, Phys. Rev. B 80 (2009) 075117.
[31] R. Funahashi, A. Kosuga, N. Miyasou, E. Takeuchi, S. Urata, K. Lee, H. Ohta, K. Koumoto, 26th International Conference on Thermoelectrics, IEEE, Piscataway, USA, 2007, p. 124.
[32] X.Y. Huang, Y. Miyazaki, T. Kajitani, Solid State Commun. 145 (2008) 132.
[33] B.T. Cong, T. Tsuji, P.X. Thao, P.Q. Thanh, Y. Yamamura, Physica B 352 (2004) 18.
[34] M.E. Melo Jorge, A. Correia dos Santos, N.M. Nunes, Int. J. Inorg. Mater. 3 (2001) 915.
[35] N.F. Mott, E.A. Davis, Electronic Processes in Non-crystalline Materials, Clarendon Press, Oxford, 1971, p. 46.
[36] F.P. Zhang, H. Peng, M.X. Wang, X. Zhang, Q.M. Lu, J.X. Zhang, 29th International Conference on Thermoelectrics, Shanghai, China, 2010, p. 103.
[37] H. Taguchi, Phys. Status Solidi A 88 (1985) K79.
[38] Y. Zhou, I. Matsubara, R. Funahashi, G. Xu, M. Shikano, Mater. Res. Bull. 38 (2003) 341.